Journal of Materials Chemistry C

Accepted Manuscript

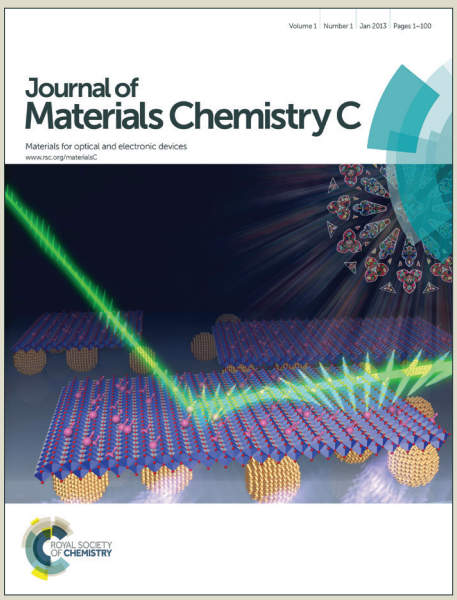

ROYAL SOCIETY OF CHEMISTRY

www.rsc.org/materialsC

Cite this: DOI: 10.1039/c0xx00000x

www.rsc.org/xxxxxx

COMMUNICATION

Fabrication of 3D ZnO hollow shell structures by prism holographic lithography and atomic layer deposition

Sung-Gyu Park,*[†a] Tae Yoon Jeon,[†b] Hwan Chul Jeon,[b] Seung-Man Yang,[b] Jung-Dae Kwon,[a] Chae-Won Mun,[a] Byungjin Cho,[a] Chang Su Kim[a] and Dong-Ho Kim[a]

Received (in XXX, XXX) Xth XXXXXXXXX 20XX, Accepted Xth XXXXXXXXX 20XX
DOI: 10.1039/b000000x

Highly uniform 3D ZnO hollow shell structures were prepared by combining prism holographic lithography (PHL) and atomic layer deposition (ALD). As a dense ZnO film was obtained by using the ALD process, no volume shrinkage occurred during the subsequent calcination to remove the sacrificial polymer template. No volume shrinkage during heat treatment is crucial for achieving excellent optical properties and mechanical stability of inverse photonic crystals (PCs).

Zinc oxide is a transparent semiconductor with a direct wide band gap (E_g = 3.37 eV). It exhibits many attractive properties such as excellent electrical conductivity, high chemical stability, low toxicity, good thermal stability, good biocompatibility, and strong piezoelectric and photoluminescence properties.[1-3] With the help of advanced nanofabrication techniques, ZnO nanostructures have been used in a wide variety of applications, including solar cells,[4-6] gas sensors,[7-9] thermoelectric devices,[10] thin-film transistors,[11,12] and piezoelectric nanogenerators.[13,14]

Much attention has been paid to ZnO-based photonic crystals (PCs) in one,[15] two,[16,17] or three dimensions.[18-20] In 3D ZnO PCs, inorganic silica or organic polystyrene opals have been dominantly used as sacrificial templates for ZnO infiltration.[18-20] As such opal templates form a close-packed system with a solid filling fraction of 74%, the maximum achievable filling fraction of frame materials after the inversion process would be 26%, which is too small for the generation of complete photonic band gaps (PBGs). Holographic lithography (HL) has the distinct advantage of being able to control the filling fraction of sacrificial polymer template by simple variation of UV exposure, with the resulting inverse structures having high filling fractions of solid material. The infiltration method adopted must be capable of filling a highly interconnected network of sub-micrometer channels, producing a dense and homogeneous network of high refractive index (RI) material. Solution-based methods such as electrodeposition[21-24] or sol–gel reactions[25] are attractive for their simplicity and ease of fabrication. Importantly, these methods allow the complete infiltration of high-RI materials into the 3D interconnected porous template, yielding 3D PCs with complete PBGs after removal of the polymer template. However, since the sol–gel process often produces mesoporous structures, a large degree of volume shrinkage and a loss of long-range structural order are likely to occur during the subsequent heat treatment.[25] In contrast to wet chemical methods, the ALD technique provides atomic-scale thickness control of films by alternating the precursors, resulting in highly conformal, dense film formation within the interconnected pores of a 3D template.[19,20,26-28] These dense films are beneficial for sustaining the integrity of the 3D inverse structures during subsequent heat treatment.

Here we present the fabrication of 3D ZnO hollow nanostructures combining the PHL and ALD techniques. Remarkably, as a highly dense ZnO film could be obtained using the ALD process, no volume shrinkage was found to occur during the subsequent calcination. Once the polymer template was inverted into the ZnO structure, the effective RI was increased, resulting in a red-shift of the reflectance peak in the normal direction. Evidence for the optical quality of the inverted PCs was

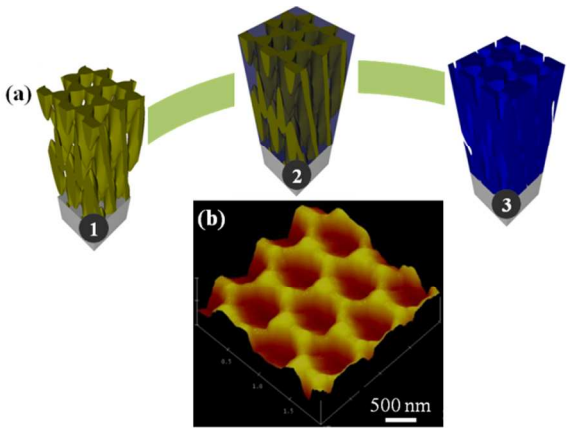

Fig. 1 (a) Schematic of the fabrication of ZnO PCs using holographically-patterned SU-8 structures. (1) Fabrication of 3D polymer template by PHL, (2) ZnO infiltration of polymer template by ALD, (3) removal of SU-8 by heat treatment at 450°C for 1 h. (b) An AFM image of 3D SU-8 templates.

[a] *Advanced Functional Thin Films Department, Korea Institute of Materials Science (KIMS), Changwon, Gyeongnam 641-831, Korea Phone: +82-55-280-3632 Fax: +82-55-280-3570 E-mail: sgpark@kims.re.kr*
[b] *National Creative Research Initiative Center for Integrated Optofluidic Systems; Department of Chemical and Biomolecular Engineering, Korea Advanced Institute of Science and Technology 335 Gwahangno, Yuseong-gu, Daejeon, 305-701 (Korea) Phone: +82-42-350-3962 Fax: +82-42-350-5962*
† These authors contributed equally to this project.

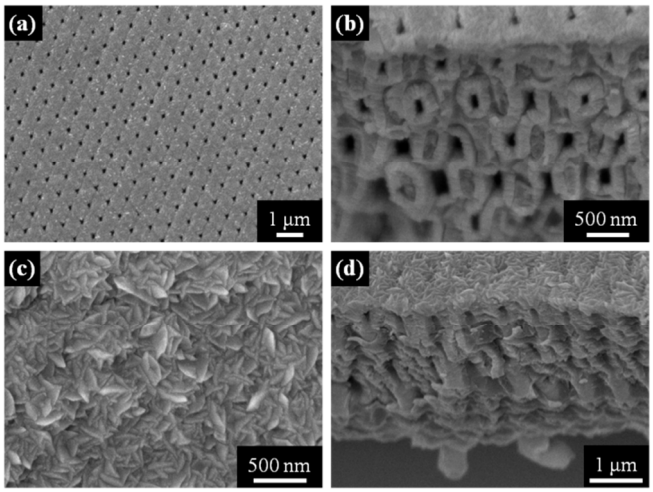

Fig. 2 SEM images of SU-8/ZnO composite at different ZnO deposition thicknesses. (a) Top view of SU-8/ZnO composite after 200 nm ZnO deposition. (b) A 45° tilted view of SU-8/ZnO composite after ALD of 200 nm ZnO, with open pores evident. (c) Top view of SU-8/ZnO composite after 400 nm ZnO deposition. Pores are closed and a rough surface is evident. (d) A 45° tilted view of SU-8/ZnO composite after 400 nm ZnO deposition.

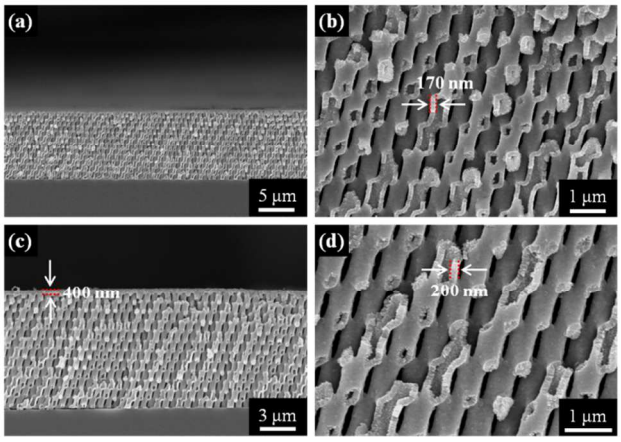

Fig. 3 (a), (b) Cross-sectional views of inverted ZnO PC formed after ALD of 200 nm ZnO, after template removal by calcination. An approximately 170 nm thick ZnO shell is apparent within the 3D porous structures. (c), (d) Cross-sectional views of inverted ZnO PC formed after ALD of 400 nm ZnO. An approximately 400 nm thick overlayer is present on the top surface. A 200 nm thick ZnO shell is evident inside the 3D porous structures.

provided by the increase in peak reflectance from the template to the final material.

The process by which 3D ZnO inverse PCs were fabricated is illustrated in Fig. 1. Firstly, an SU-8 polymer template with face-centered cubic (fcc) symmetry was obtained using PHL (Fig. 1a-1). The SU-8 photoresist (PR) was prepared by mixing the SU-8 resin (150 wt% to solvent) and a cationic photoacid generator (PAG, triarylsulfonium hexafluorophosphate, 1.3 wt% to resin) in solvent (gamma-butyrolactone (GBL)). A detailed description of the optical setup used and the specially designed prism can be found in previous reports.[29-33] A layer of PR approximately 10 μm thick was obtained by spin-casting the solution onto a glass substrate, followed by soft baking at 95°C to evaporate the solvent. A laser beam (HeCd laser, 325 nm, 50 mW, Kimmon, beam diameter 1 mm) was subsequently passed through a beam expander and directed perpendicularly to a top-cut fused silica prism. A low temperature (55°C) post-exposure bake was then performed in order to relieve the thermal stress built up during the development process. Finally, unexposed regions were removed using propylene glycol methyl ether acetate (PGMEA, Aldrich), and the sample was then rinsed with 2-propanol. The HL-patterned SU-8 templates were then filled with ZnO using ALD (Fig. 1a-2). The ZnO films were deposited at 100°C by using an ALD system [Lucida M100, NCD]. Diethyl zinc (DEZ, $Zn(C_2H_5)_2$) and deionized water vapor were used as the zinc precursor and oxygen source, respectively.[34,35] The temperature of the DEZ source was maintained at 10°C using a cooling circulator. The canister containing the water source was held at room temperature. During deposition, argon gas was continuously flowed through the reaction chamber at a rate of 100 sccm. ALD technique provides atomic-scale thickness control of films, as a result of self-limited surface reaction.[19] ALD growth rate is usually expressed in terms of thickness increment per cycle, e.g., nanometers per cycle or angstroms per cycle. Normally, the growth rate is determined after the film growth by dividing the measured film thickness by the number of deposition cycles applied. The thickness per cycle of the ZnO ALD layer was 1.39 Å/cycle. The number of ALD cycles was regulated in order to achieve ZnO thin films with predefined thicknesses. Calcination at 450°C was performed for 1 h in order to decompose the crosslinked SU-8 material (Fig. 1a-3). A slow temperature ramp is important for maintaining structural integrity before removal of the polymer template to prevent film collapse. To this end, we selected a slow temperature ramp rate of 1°C/min for this calcination step. The morphologies of the top surfaces and cross-sections of the Au-deposited 3D ZnO nanostructures were investigated using field emission-scanning electron microscopy (FE-SEM, Hitachi S-4800). The surface topography was evaluated using AFM (XE-100, CNUCRF). The root mean square (rms) of the surface roughness was obtained from the AFM images. Fig. 1b shows an atomic force microscopy (AFM) image of a prepared 3D SU-8 template. The SU-8 structures can be seen to consist of a network of interconnected pores arranged into an fcc lattice, with a lattice constant of 650 nm and a pore size of 500 nm at the top surface. Compared to other holographically-defined SU-8 templates, that described here, exhibited a five-fold increase in the size of the pores on the top surface.[26] In the case of gas phase reactions such as that which occurs in ALD, the deposition is terminated by closure of the top pore channels, thus, a five-fold increase in the top pore size is highly beneficial for generating inverse structures with a high filling fraction.[26] Enabling a high level of infiltration of the high RI material is crucial for achieving excellent optical properties and mechanical stability. The holographically-patterned 3D SU-8 structures can be seen to have a smooth surface, with the rms roughness calculated to be 8.5 nm.

Fig. 2a and b show SEM images of the prepared ZnO/SU-8 composite with 200 nm deposition of ZnO. It is evident that a highly uniform and conformal film was produced on the polymer template. The size of the pores on the top layer decreased to about 100 nm from 500 nm, with 200 nm deposition of ZnO. In the case of gas phase reactions such as that which occurs in ALD,

Table 1 Optical properties and filling fraction of the SU-8 and ZnO PCs.

PCs	Reflectance peak position (μm)	Interlayer spacing along [111] direction (nm)	Reflectance (%)	Filling fraction of skeleton material (%)
SU-8/air	1.99	750	29	44
SU-8/ZnO/air composite	2.60	750	28	SU-8=44, ZnO=46
ZnO (200 nm)/air	2.20	750	47	42
ZnO (400 nm)/air	2.23	750	41	44

the deposition is terminated by closure of the top pore channels, which leads to incomplete infiltration of the high RI material. With the 400 nm deposition of ZnO, the top pores became closed, and a rough surface was formed (Fig. 2c and d). However, even after this level of deposition, complete infiltration of the pores was not achieved due to pinch-off problems.[36,37]

Fig. 3 presents cross-sectional SEM images of the ZnO PCs after the calcination process. It should be noted that the lattice parameters of the inverse structures match those of the polymer template. Remarkably, as a highly dense ZnO film was obtained from the ALD process, anisotropic volume shrinkage did not occur during the calcination. Moreover, a slow temperature ramp of 1°C/min relieved the thermal stress in the 3D composite ZnO/SU-8 structures during the heating process.[25] This is in contrast to the use of a sol–gel process, where a large degree of volume shrinkage (over 30%) occurs during the heat treatment, which is due to production of a mesoporous structure.[25] We previously reported that electrodeposited Cu_2O inverse PCs did not suffer from volume shrinkage during inversion due to the low temperature (65°C) at which the process was carried out.[23,24] In the present work, ZnO hollow shell morphologies were formed inside the 3D porous structures, regardless of the ZnO deposition thickness. A 170 nm thick shell was formed with 200 nm deposition of ZnO; while, for 400 nm of ZnO deposition, a shell that was only 30 nm thicker was produced (Fig. 3b and d). Once the top channels became closed, the gas phase ZnO precursor was not able to penetrate into the pores of the ZnO/SU-8 composite, which lead to termination of shell growth. The ZnO thickness on the top layer was well matched to that of the deposition thickness (Fig. 3c).

Fig. 4 presents the optical properties of the ZnO inverse structures with different ZnO deposition thicknesses. Once 200 nm thick ZnO was deposited onto SU-8 template, the effective RI was increased, resulting in a red-shift of the reflectance peak in the normal direction. Compared to SU-8 template, the reflectance peak was red-shifted to ~2.6 μm in the SU-8/ZnO composite. From the reflectance peak position, the effective RI for the SU-8/ZnO composite is estimated to be 1.73, based on Bragg's Law.[29] The filling fraction of the as-deposited polycrystalline ZnO (assuming the RI for the polycrystalline ZnO is 1.93) is calculated to be 46% (while filling fraction of SU-8 and air are assumed to be 44% and 10%, respectively), which agrees reasonably well with the filling fraction (42%) of 3D ZnO inverse structures after calcination (Table 1). Since ALD provides incomplete infiltration of ZnO into the polymer template, the volume fraction of air in the SU-8/ZnO composite should be considered when calculating volumetric filling fraction of ZnO in the SU-8/ZnO composite. Even though there is small discrepancy (46% vs. 42%) in calculated filling fraction of ZnO between SU-8/ZnO composite and ZnO/air inverse PCs, we can conclude that no volume shrinkage occurred during the heat treatment. We think small discrepancy in calculated filling fraction of ZnO between SU-8/ZnO/air composite and final ZnO/air inverse

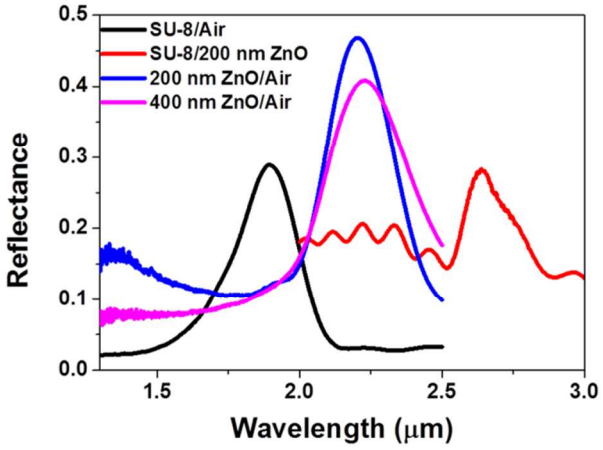

Fig. 4 Reflectance spectra of the 3D PCs.

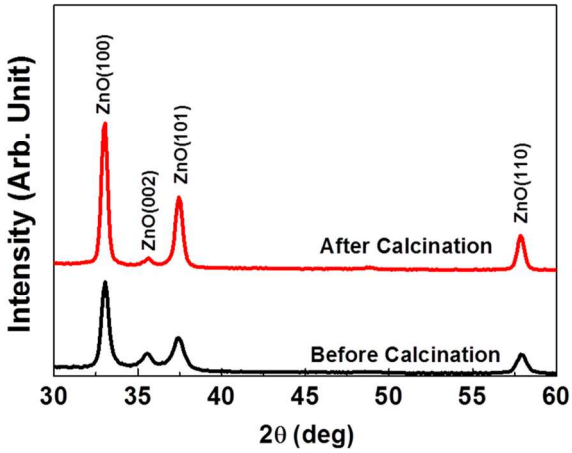

Fig. 5 XRD diffraction pattern of the ZnO film before and after calcination at 450°C for 1 h, indicating the polycrystalline nature of ZnO, regardless of calcination.

structures may be due to the three component systems of SU-8/ZnO/air composite, resulted from incomplete infiltration of ZnO into the polymer template. After calcination to remove the SU-8 polymer template, the reflectance peak of the 3D ZnO inverse PCs blue-shifted to ~ 2.2 μm. Evidence for the optical quality of the inverted PCs is provided by the increase in peak reflectance from 29% for the SU-8 template to 47% for the 200 nm thick ZnO/air structure (Table 1). Since the rough top layer of the ZnO was not smoothened by post-processing steps, including reactive-ion etching or polishing, the peak reflectance was relatively low in comparison to other high RI inverse structures that have been previously reported.[22-24] Both a high degree of structural order and a smooth surface are crucial for achieving high quality PCs. With the 400 nm of ZnO deposition, the peak position was slightly red-shifted, while peak reflectance was decreased to 41%. This can be attributed to the generation of a rougher surface. Normally, as the film grows thicker the crystallites become larger, and then the surface roughness increases.[38,39] The formation of an overcoat can significantly diminish the optical properties of ZnO inverse structures, owing to random scattering caused by high surface roughness of the bulk layer.[23] Assuming the RI for the polycrystalline ZnO is 1.93 (Fig. 5),[18] the volumetric filling fractions of ZnO for 200 nm and 400 nm deposition were calculated to be 42% and 44%, respectively. These values are much higher than the theoretical filling fraction (26%) achieved using inverse opal templates. Considering the volume fraction (56%) of air in the SU-8 template, incomplete infiltration of ZnO into the polymer template through the gas-phase reaction was achieved (Table 1).

Figure 5 presents the XRD spectra of the ZnO films before and after calcination. The XRD spectra indicated that all ZnO films were polycrystalline wurtzite structures regardless of calcination. ZnO films easily crystallize at low deposition temperature of 100 °C.[35] After calcination, the stronger peaks observed at the diffraction of the (100) and (101) planes of ZnO. It means that the ZnO grains with (100) and (101) planes were grown by thermal energy.

In summary, 3D ZnO inverse PCs were prepared by combining PHL and ALD. Remarkably, no anisotropic volume shrinkage occurred during the calcination process, providing beneficial optical properties and mechanical stability. These 3D ZnO hollow shell structures can be used for highly efficient gas sensors by utilizing high porosity and large surface area.

Acknowledgements

This work was supported by the research fund of the Korea Institute of Materials Science. This work was also supported by the "Gyeongsangnam, Changwon Science Research Park Project" of the Grant of the Korean Ministry of Science, ICT and Future Planning. The authors thank to CNUCRF for supporting AFM (XE-100, Parks Systems Corp.) measurements

Notes and references

1. U. Ozgur, Y. I. Alivov, C. Liu, A. Teke, M. Reshchikov, S. Dogan, V. Avrutin, S. -J. Cho and H. Morkoc, *J. Appl. Phys.,* 2005, **98**, 041301.
2. A. Wei, L. Pan and W. Huang, *Mater. Sci. Eng. B,* 2011, **176**, 1409-1421.
3. Z. L. Wang, *Appl. Phys. A,* 2007, **88**, 7-15.
4. I. Repins, M. A. Contreras,B. Egaas, C. DeHart, J. Scharf, C. L. Perkins, B. To and R. Noufi, *Prog. Photovoltaics Res. Appl.,* 2008, **16**, 235-239.
5. K. Keis, E. Magnusson, H. Lindstrom, S.-E. Lindquist and A. Hagfeldt, *Sol. Energy Mater. Sol. Cells,* 2002, **73**, 51-58.
6. A. K. K. Kyaw, D. H. Wang, D. Wynands, J. Zhang, T.-Q. Nguyen, G. C. Bazan and A. J. Heeger, *Nano Lett.,* 2013, **13**, 3796-3801.
7. X. Liu, J. Zhang, L. Wang, T. Yang, X. Guo, S. Wu, and S. Wang, *J. Mater. Chem.,* 2011, **21**, 349-356.
8. J. Xu, Q. Pan, Y. A. Shun and Z. Tian, *Sens. Actuators B, 2*000, **66**, 277-279.
9. L. Wang, Y. Kang, X. Liu, S. Zhang, W. Huang, and S. Wang, *Sens. Actuators B,* 2012, **162**, 237-243.
10. P. Jood, R. J. Mehta, Y. Zhang, G. Peleckis, X. Wang, R. W. Siegel, T. Borca-Tasciuc, S. X. Dou and G. Ramanath, *Nano Lett.,* 2011, **11**, 4337-4342.
11. E. M. C. Fortunato, P. M. C. Barquinha, A. Pimentel, A. M. F. Gozalves, A. J. S. Marques, L. M. N. Pereira and R. F. P. Martins, *Adv. Mater.,* 2005, **17**, 590-594.
12. P. F. Carcia, R. S. McLean, M. H. Reilly and G. Nunes, *Appl. Phys. Lett.,* 2003, **82**, 1117-1119.
13. Z. L. Wang and J. Song, *Science,* 2006, **312**, 242-246.
14. P. X. Gao, J. Song, J. Liu and Z. L. Wang, *Adv. Mater.,* 2007, **19**, 67-72.
15. H.-Y. Lee and T. Yao, *J. Appl. Phys.,* 2003, **93**, 819-830.
16. X. D. Wang, C. Neff, E. Graugnard, Y. Ding, J. S. King, L. A. Pranger, R. Tannenbaum, Z. L. Wang and C. J. Summers, *Adv. Mater.,* 2005, **17**, 2103-2106.
17. M. Matsuu, S. Shimada, K. Masuya, S. Hirano and M. Kuwabara, *Adv. Mater.,* 2006, **18**, 1617-1621.
18. B. H. Juárez, P. D. García, D. Golmayo, A. Blanco and C. López, *Adv. Mater.,* 2005, **17**, 2761-2765.
19. M. Scharrer, X. Wu, A. Yamilov, H. Cao, R. P. H. Chang, *Appl. Phys. Lett.,* 2005, **86**, 151113.
20. J. S. King, C. W. Neff, C. J. Summers, W. Park, S. Blomquist, E. Forsythe and D. Morton, *Appl. Phys. Lett.,* 2003, **83**, 2566-2568.
21. P. V. Braun and P. Wiltzius, *Adv. Mater.,* 2001, **13**, 482-485.
22. Y. Xu, X. Zhu, Y. Dan, J. H. Moon, V. W. Chen, A. T. Johnson, J. W. Perry and S. Yang, *Chem. Mater.,* 2008, **20**, 1816-1823.
23. S.-G. Park, M. Miyake, S.-M. Yang and P. V. Braun, *Adv. Mater.,* 2011, **23**, 2749-2752.
24. M. Miyake, Y.-C. Chen, P. V. Braun and P. Wiltzius, *Adv. Mater.,* 2009, **21**, 3012-3015.
25. S.-G. Park, T. Y. Jeon and Yang, S.-M., *Langmuir,* 2013, **29**, 9620-9625.
26. J. S. King, E. Graugnard, O. M. Roche, D. N. Sharp, J. Scrimgeour, R. G. Denning, A. J. Turberfield and C. J. Summers, *Adv. Mater.,* 2006, **18**, 1561-1565.
27. A. Frölich, J. Fischer, T. Zebrowski, K. Busch and M. Wegener, *Adv. Mater.,* 2013, **25**, 3588-3592.
28. J. S. Daniel, C. N. Erik, C. Debashis, B. Andrew, V. B. Paul, A. R. John, W. Pierre, *J. Vac. Sci. Technol. B,* 2010, **28**, 783-788.

29. S. K. Lee, S. G. Park, J. H. Moon and S. -M. Yang, *Lab Chip*, 2008, **8**, 288-391.
30. S.-G. Park, S. K. Lee, J. H. Moon and S.-M. Yang, *Lab Chip*, 2009, **9**, 3144-3150.
31. S.-G. Park, J. H. Moon, S.-K. Lee, J. Shim and S.-M. Yang, *Langmuir,* 2009, **26**, 1468-1472.
32. S.-G. Park, J. H. Moon, H. C. Jeon and S.-M. Yang, *Soft Matter,* 2012, **8**, 4567-4570.
33. J.-H. Kang, J. H. Moon, S.-K. Lee, S.-G. Park, S. G. Jang, S. Yang and S.-M. Yang, *Adv. Mater.,* 2008, **20**, 3061-3065.
34. J.-D. Kwon, J.-W. Lee, K.-S. Nam, D.-H. Kim, Y. Jeong, S.-H. Kwon and J.-S. Park, *Curr. Appl Phys.,* 2012, **12**, S134-S138.
35. T.-H. Jung, J.-S. Park, D.-H. Kim, Y. Jeong, S.-G. Park, J.-D. Kwon, *J. Vac. Sci. Technol. A,* 2013, **31**, 01A1241-01A1244.
36. J. H. Moon, Y. G. Xu, Y. P. Dan, S. -M. Yang, A. T. Johnson and S. Yang, *Adv. Mater.,* 2007, **19**, 1510-1514.
37. J. H. Moon, S. Yang, W. T. Dong, J. W. Perry, A. Adibi and S. M. Yang, *Opt. Express,* 2006, **14**, 6297-6302.
38. S. A. Catledge, W. Comer and Y. K. Vohra, Appl. Phys. Lett., 1998, 73, 181-183
39. M. E. Alnes, E. Monakhov, H. Fjellvag and O. Nilsen, Chem. Vap. Dep., 2012, 18, 173-178